Viscosity-dependent flow reversal in a density oscillator

T. Kano* and S. Kinoshita
Graduate School of Frontier Biosciences, Osaka University, Suita 565-0871, Japan
(Received 27 March 2007; revised manuscript received 26 July 2007; published 8 October 2007)

The density oscillator is a simple system that exhibits self-sustained oscillation. It alternately exhibits up and down flow through a pipe which connects two containers filled with fluids of different densities. However, the mechanism of the flow reversal has not yet been fully understood. From the detailed measurements, we have found that flow reversal begins with an intrusion of fluid, which is followed by rapid growth. This process is definitely sensitive to the viscosities of the fluids, and as a consequence, the critical heights leading to flow reversal are clearly viscosity dependent. These experimental results are explained by a simple model, derived by considering forces acting on a unit volume element located at the tip of the intrusion. Using this model, we can successfully explain the mechanism of flow reversal, which is the most essential process in a density oscillator.

DOI: 10.1103/PhysRevE.76.046208 PACS number(s): 05.45.−a, 82.40.Bj, 05.90.+m

I. INTRODUCTION

Self-sustained oscillation is an extremely important phenomenon in nature and has been extensively studied from physical, chemical, biological, and technological viewpoints. Neural spiking, circadian rhythms, gene expression, Belousov-Zhabotinsky reaction, and Josephson junction arrays are some well-known examples [1–6]. A self-oscillatory system draws a limit cycle in phase space and exhibits a wide variety of behaviors, such as the bifurcation of oscillatory modes and entrainment between oscillators, which causes various types of synchronization [7,8]. In particular, when the limit cycle is characterized by more than two different time scales, the oscillator is called a "relaxation-type oscillator," and it is known to be highly nonlinear and dissipative [8,9].

The density oscillator is a typical example of a relaxation-type oscillator [10–20]. Because of the simplicity in its experimental setup, it provides an excellent way to investigate the essential mechanism of relaxation-type oscillation. The density oscillator usually consists of an inner container with a thin pipe attached at the bottom, which is held within an outer container. The inner container is filled with heavy fluid, while the outer container is filled with light fluid. When the surfaces of both fluids are initially set at nearly the same height, the heavy fluid starts to flow downward through the pipe, owing to the gradient of hydrostatic pressure. At a critical height, the flow loses stability and flow reversal occurs, which causes the light fluid to flow upward through the pipe. At another critical height, the flow loses stability again, causing flow reversal and leading the heavy fluid to flow downward. In this way, the oscillation continues for more than several tens of cycles.

A quantitative study of the density oscillator was performed by Martin in 1970 [10]. He analyzed the up and down flow inside the pipe according to Poiseuille's law, and showed that the experimental result was well explained by his analysis. On this basis, Yoshikawa *et al.* derived a phenomenological equation [11–13] and explained a wide variety of behaviors [11,12]. Later, Okamura *et al.* confirmed the validity of this model with a simulation study [14]. Another interesting topic related to the density oscillator is the entrainment among multiple oscillators, which is observed when multiple inner containers are held within an outer container [12,15–18]. Nakata *et al.* investigated the fluid-surface dependence of the synchronization [15], while Yoshikawa *et al.* [12] and Miyakawa and Yamada [16] reported coupling among 3 and 36 oscillators, respectively. Miyakawa and Yamada also reported a system consisting of two oscillators coupled with one another through the window of the partition wall [17].

Although the phenomenological behavior of the density oscillator has been extensively studied as described above, the essential cause of the flow reversal has not been fully discussed and has been considered to be due to Rayleigh-Taylor instability [10]. However, the dynamical process of the flow reversal cannot be understood in terms of Rayleigh-Taylor instability, because Rayleigh-Taylor instability is only applicable to a static interface between two fluids [21]. In fact, the spatiotemporal dynamics during flow reversal are much more complex and are known to proceed in the following way [10,19,20]: In down to up flow, for instance, the flow reversal initiates from an intrusion of light fluid along the inner wall of the pipe. After some time, the intrusion begins to grow rapidly and climbs to the upper end of the pipe, and then the flow reverses completely (see Fig. 9). Steinbock *et al.* analyzed the stability of the down flow inside the pipe, and derived the critical height for the instability of the flow [19]. The critical height thus obtained was in good agreement with their experiment, when either the density of heavy fluid or the pipe length was varied. However, they did not take into account the flow after it passes through the pipe. In addition, the temporal evolution of the dynamical behavior during the flow-reversal process was not considered, since the steady-state approximation was employed in their analysis. Thus, the mechanism of the flow reversal is still not completely understood.

From a hydrodynamic point of view, fluid dynamics in a system consisting of two viscous fluids has been an intriguing problem [22,23]. Interestingly, the dynamics are known

*takesik@fbs.osaka-u.ac.jp

to be extremely sensitive to the viscosities of the fluids. One of the well-known examples is Saffman-Taylor instability, where an interface between two fluids tends to become unstable when less viscous fluid is forced into more viscous fluid in a porous medium or a Hele-Shaw cell, while it remains stable in the opposite case [22].

Thus, it is strongly expected that even in a density oscillator, the dynamical behavior inside a connecting pipe will be largely affected by the viscosities of the fluids. Hence, the study of viscosity-dependent phenomena is essential to fully understanding the flow-reversal process and hence the fundamental mechanisms of the density oscillator. In the present paper, we will show that the behavior of the flow reversal and the critical heights at flow reversal are extremely sensitive to the viscosities of the fluids. Finally, we will propose a simple model to explain the mechanism involved.

II. THEORETICAL BACKGROUNDS

First, we will briefly review the theories proposed so far to explain the phenomenon of density oscillation. Martin [10] constructed a model to describe the time courses of up and down flow in a density oscillator based on the Navier-Stokes equation under the assumption that Poiseuille's law is operative inside the pipe. Each flow is then described by the following equation:

$$\frac{d^2X}{d\tau^2} + \frac{2\sigma_i^{1/2}}{\beta}\left[\frac{\nu_H}{\nu_L}\frac{dX}{d\tau} - \frac{\sigma_i^{1/2}\beta}{4}\left(\frac{dX}{d\tau}\right)^2\right] + \sigma_i X = 0$$

$$\text{for } \frac{dX}{d\tau} < 0, \tag{1}$$

$$\frac{d^2X}{d\tau^2} + \frac{2\sigma_i^{1/2}}{\beta}\left[\frac{dX}{d\tau} + \frac{\sigma_i^{1/2}\beta}{4}\left(\frac{dX}{d\tau}\right)^2\right] + \sigma_i(X-1) = 0$$

$$\text{for } \frac{dX}{d\tau} > 0, \tag{2}$$

where $X=(x-x_{de}^{(i)})/(\delta\rho^{(i)}d/\rho_L)$, $\tau=4\nu_L\beta t/(a^2\sigma_i^{1/2})$, $\beta^2=ga^6\pi/(16S_{\text{in}}\nu_L^2 d)$, $\sigma_i=3S_{\text{in}}\delta\rho^{(i)}/(2\pi a^2\rho_L)$, $\nu_H=\mu_H/(\rho_L+\delta\rho^{(i)})$, and $\nu_L=\mu_L/\rho_L$ with x, t, a, d, and S_{in}, the height of the heavy fluid surface, the time, the radius of the pipe, the pipe length, and the surface area of the inner container, respectively, while ρ_L, μ_H, and μ_L are the density of the light fluid, and the viscosities of the heavy and light fluids, respectively (see Fig. 1). The surface area of the outer container is assumed to be sufficiently large compared with that of the inner container. $x_{de}^{(i)}$ is the value of x at a hydrostatic equilibrium for a pipe filled with heavy fluid at the ith cycle, and $\delta\rho^{(i)}$ is the difference in densities between the heavy and light fluid at down flow of the ith cycle [24], where the term "cycle" is defined as a sequence of down and up flow. It is noticed that Eqs. (1) and (2) have asymptotic values of $X=0$ and 1, which correspond to hydrostatic equilibria for a pipe filled completely with heavy and light fluids, respectively. Actually, it has been experimentally confirmed that the time courses during the up and down flow are well expressed by Eqs. (1) and (2). However, the oscillatory behavior cannot be introduced into these equations, because the flow reversal, i.e., switching between Eqs. (1) and (2), is not taken into account.

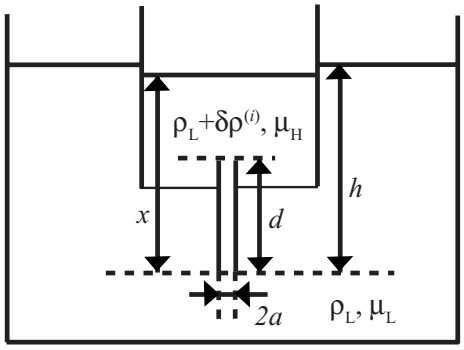

FIG. 1. Definition of the parameters. a and d are the radius and length of a pipe, while x and h are the heights of the heavy and light fluid surfaces, respectively. ρ_L is the density of the light fluid and $\delta\rho^{(i)}$ is the difference in densities between the heavy and light fluids at down flow of the ith cycle. μ_H and μ_L are the viscosities of the heavy and light fluids, respectively.

Yoshikawa *et al.* derived a simple relation for this system by combining Eqs. (1) and (2) under an assumption of $\nu_H \approx \nu_L$ and by expanding it to the third order of $\dot{X}$ as follows [11–13]:

$$\ddot{X} + C_1\dot{X}^3 - C_2\dot{X} + \omega^2 X = 0, \tag{3}$$

where C_1, C_2, and ω are positive constants. Equation (3) has become one of the most common qualitative descriptions of oscillatory behaviors.

Although Eqs. (1)–(3) characterize the behaviors of the density oscillator fairly well, the flow-reversal process is not described explicitly either from a phenomenological or microscopic standpoint. On the contrary, Steinbock *et al.* focused on the flow-reversal process [19]. They analyzed the stability of the down flow inside the pipe using a one-fluid model in a two-dimensional geometry. Using fundamental equations of hydrodynamics and the diffusion equation under a steady-state approximation, they derived a simple equation for the critical height of the heavy fluid surface x_c, where the instability of the down flow was considered to occur according to the following relation:

$$x_c - x_{de} = \frac{1}{6}\frac{\delta\rho}{\rho_L + \delta\rho}d. \tag{4}$$

Since x_{de} does not depend on the viscosities of the fluids, the critical height of the flow instability is essentially invariant against the change of the viscosity. In the following sections, we will show that it is extremely sensitive to the viscosities of the fluids. Thus, the modification of the theoretical model is inevitable.

III. EXPERIMENTAL PROCEDURES

The experimental setup is shown in Fig. 2. The density oscillator employed here consisted of an inner and an outer

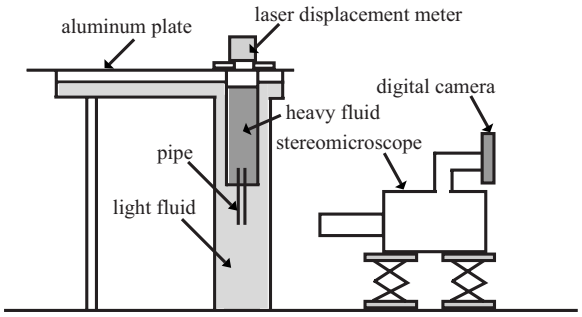

FIG. 2. Experimental setup. The inner and outer containers are filled with heavy and light fluids, respectively. A glass pipe is fixed at the bottom of the inner container.

container, whose surface areas were 7.70×10^{-4} m^2 and 5.34×10^{-2} m^2, respectively. The surface area of the inner container was sufficiently small compared with that of the outer container. The heights of the inner and outer containers were 0.15 and 0.32 m, respectively. A glass pipe whose internal diameter and length were 0.73 and 70 mm, respectively, was fixed at the bottom of the inner container. The inner container was filled with heavy fluid, and the outer container with light fluid, both of which were mixtures of water, one-propanol, and glycerin. By changing their composition, the viscosities of the fluids could be varied while maintaining their densities, as shown in Fig. 3. The densities of the heavy and light fluids were set to be constant at $(1.057\pm0.003)\times10^3$ kg m^{-3} and $(0.996\pm0.003)\times10^3$ kg m^{-3}, respectively, and hence the difference in densities between the fluids was $(0.061\pm0.004)\times10^3$ kg m^{-3}. The viscosity of the solution was measured by an Ostwald viscosimeter. In order to remove air bubbles, water mixed into the fluids was boiled before use. At the beginning of the experiments, we set the heights of the heavy and light fluid surfaces to be nearly equal, so that the oscillation began with down flow.

Throughout the experiments, the inner and outer containers were covered with an aluminum plate to prevent evaporation. The height of the heavy fluid surface was monitored by a laser displacement meter (Hokuyo, PDA-03KT), while the lower part of the glass pipe was observed simultaneously by a stereomicroscope equipped with an Olympus DP70 digital camera. The interface of the two fluids was clearly observed owing to the difference in their refractive indices. The temperature of the experimental system was maintained at 25.0±0.5 °C.

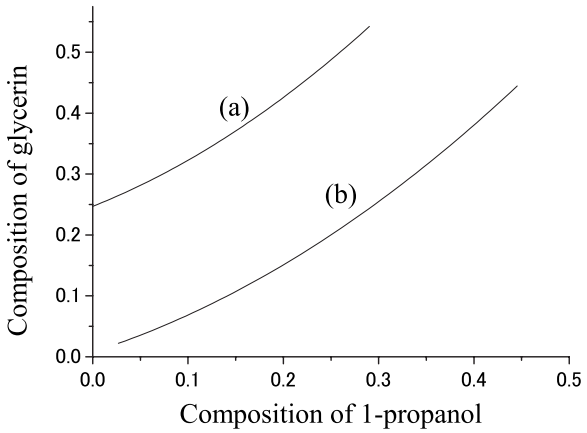

FIG. 3. The composition curve of one-propanol, glycerin, and water to give a constant density of (a) 1.057×10^3 kg m^{-3} and (b) 0.996×10^3 kg m^{-3}. The sum of the weights of the three compositions is set to be unity.

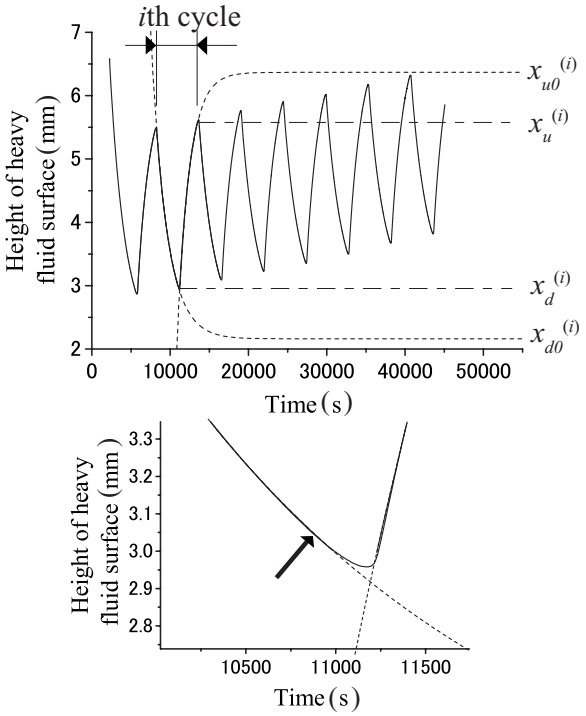

FIG. 4. Temporal evolution of the height of the heavy fluid surface. Each branch for up and down flow is well fitted by an exponential curve (dashed line). $\rho_L=0.997\times10^3$ kg m^{-3}, $\delta\rho=0.062\times10^3$ kg m^{-3}, $\mu_H=2.64\times10^{-3}$ Pa s, and $\mu_L=1.98\times10^{-3}$ Pa s. The definition of the parameters for the ith cycle is also shown. The dashed and dotted lines denote the height at which the flow reverses from the ith up flow to the $(i+1)$th down flow and from the ith down flow to the ith up flow. In the present graph, $i=2$. The lower graph shows a magnified view of the upper graph at the flow reversal from down to up flow. An arrow denotes the height of the heavy fluid surface when the intrusion length becomes 1 mm.

IV. EXPERIMENTAL RESULTS

First, we show the temporal evolution of the height of the heavy fluid surface measured by the laser displacement meter. Figure 4 shows the case where the viscosities of the heavy and light fluids are not extremely high compared with pure water. It is found that the fluid surface regularly moves up and down in a range of ~2.5 mm within a period of ~5000 s. The amplitude and period are kept almost constant for at least ten cycles, while the average height shows a slow but continuous increase. This is because the accumulation of the light fluid into the inner container causes a periodic decrease in the density of the heavy fluid. As the number of

cycles increases, the amplitude and increasing rate of the average height gradually decrease because of the reduction in the average difference in densities, and finally, the oscillation stops.

Next, let us turn our attention to each up and down flow. It is found that the temporal evolution for each flow between two adjacent flow reversals can be expressed by an exponential function. This is because the nonlinear terms proportional to $\dot{X}^2$ and the inertia terms in Eqs. (1) and (2) are negligible, since the coefficients of the viscous terms proportional to $\dot{X}$ are more than 66 times as large as those of the nonlinear and inertia terms, estimated using the following parameters: $\beta=4.62\times10^{-3}$, $\sigma=1.71\times10^{2}$, $\nu_H=2.50\times10^{-6}$ m^2 s^{-1}, and $\nu_L=1.99\times10^{-6}$ m^2 s^{-1}. Thus, Eqs. (1) and (2) are solved analytically as

$$X = C_d e^{-t/\tau_d} \quad \text{for } \frac{dX}{d\tau} < 0 \tag{5}$$

and

$$X = 1 - C_u e^{-t/\tau_u} \quad \text{for } \frac{dX}{d\tau} > 0, \tag{6}$$

where $\tau_d=\nu_H r$ and $\tau_u=\nu_L r$ with $r\equiv 8S_{\text{in}}d/(a^4 g\pi)$, and C_d and C_u are positive constants. In the present experimental condition, τ_d and τ_u are estimated to be 1.97×10^3 s and 1.57×10^3 s, which are in good agreement with the experimental results of 1.99×10^3 s and 1.58×10^3 s, respectively.

Now, we consider the difference between the asymptotic values of the two adjacent exponential functions. As described above, the asymptotic values for Eqs. (2) and (1) correspond to the hydrostatic equilibria for a pipe filled with light and heavy fluids, respectively. The heights of the heavy fluid surfaces at these equilibria are derived from the following simple hydrostatic balances under the assumption that the average difference in densities of the fluids at the asymptotic value of $(i-1)$th up flow is approximately $\delta\rho^{(i)}$:

$$(\rho_L + \delta\rho^{(i)})(x_{ue}^{(i-1)} - d) \approx \rho_L(h-d), \tag{7}$$

$$(\rho_L + \delta\rho^{(i)})x_{de}^{(i)} = \rho_L h, \tag{8}$$

where h is the height of the light fluid surface in the outer container measured from the lower end of the pipe, and $x_{ue}^{(i-1)}$ is the value of x at a hydrostatic equilibrium for a pipe filled with light fluid at the $(i-1)$th cycle. Thus, the difference between the up flow at the $(i-1)$th cycle and the down flow at the ith cycle $\delta x^{(i)}$ is derived as

$$\delta x^{(i)} = x_{ue}^{(i-1)} - x_{de}^{(i)} \approx \frac{\delta\rho^{(i)} d}{\rho_L + \delta\rho^{(i)}}. \tag{9}$$

In the present experimental condition, δx becomes 4.09 mm for $\delta\rho=0.062\times10^3$ kg m^{-3}, where it is assumed that $\delta\rho$ does not vary significantly throughout several oscillation cycles. From our experiment, the difference between the asymptotic values for the up flow at the $(i-1)$th cycle and the down flow at the ith cycle $\Delta^{(i)}$ is found to be 4.10 mm, obtained by averaging over four cycles from the second to the fifth, which is also in good agreement with the theoretical expectation of δx. Thus, without the flow-reversal process, the overall behavior of the density oscillator is quantitatively describable using Eqs. (1) and (2).

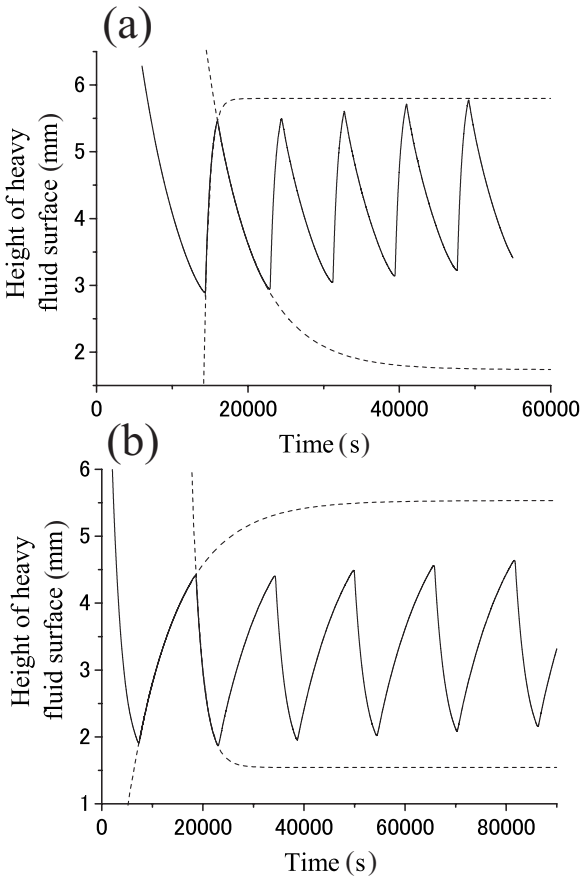

FIG. 5. Temporal evolution of the height of the heavy fluid surface, in the case of (a) $\rho_L=0.997\times10^3$ kg m^{-3}, $\delta\rho=0.060\times10^3$ kg m^{-3}, $\mu_H=8.59\times10^{-3}$ Pa s, and $\mu_L=0.89\times10^{-3}$ Pa s, and (b) $\rho_L=0.996\times10^3$ kg m^{-3}, $\delta\rho=0.062\times10^3$ kg m^{-3}, $\mu_H=2.66\times10^{-3}$ Pa s, and $\mu_L=14.18\times10^{-3}$ Pa s. Each branch for up and down flow is well fitted by an exponential curve (dashed line).

When the viscosity of the fluid is varied, the oscillatory behavior changes drastically. Figure 5 shows examples of the temporal evolutions in the case of extremely high viscosity applied to the heavy or light fluid. As is expected, the time constant of the exponential curve varies according to the viscosity of the fluid, although the difference between the asymptotic values for the exponential curves Δ is still almost consistent with δx, as shown in Fig. 6. Figure 7 shows the time constants of the exponential curves fitted for the up and down flow. The experimental results are also in fairly good agreement with the theoretical values τ_u and τ_d obtained from Eqs. (2) and (1), although there is a slight systematic deviation at high viscosity, which is thought to be caused by the reduction in the viscosity of the high viscosity fluid due to the inflow of the low viscosity fluid. Thus, even when the viscosity of the light or heavy fluid is varied, each branch for the up and down flow is well described by Eqs. (2) and (1).

However, when we compare Fig. 5 with Fig. 4, we notice that a drastic change occurs at the timing of the flow reversal. In order to evaluate it quantitatively, we have defined the two parameters s_d and s_u as

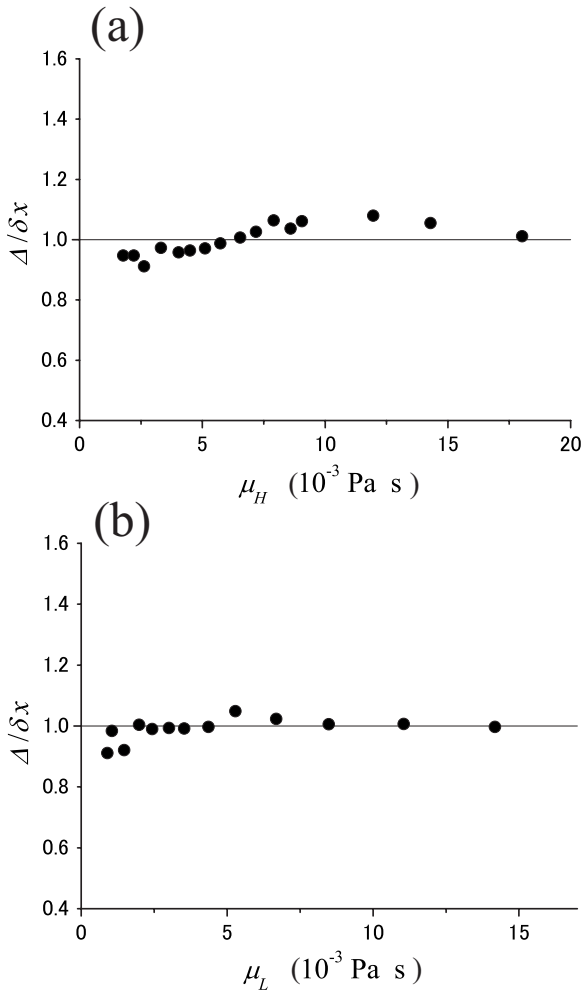

FIG. 6. The ratio of Δ to δx. The data are averaged over four cycles from the second to the fifth. (a) μ_H is varied while μ_L is fixed at 0.89×10^{-3} Pa s. (b) μ_L is varied while μ_H is fixed at $(2.63\pm0.03)\times10^{-3}$ Pa s. Although the viscosities of the fluids are varied, Δ almost agrees with δx.

$$s_d = \left\langle \frac{x_d^{(i)} - x_{d0}^{(i)}}{x_{u0}^{(i-1)} - x_{d0}^{(i)}} \right\rangle,$$

$$s_u = \left\langle \frac{x_u^{(i-1)} - x_{d0}^{(i)}}{x_{u0}^{(i-1)} - x_{d0}^{(i)}} \right\rangle, \tag{10}$$

where $x_d^{(i)}$ and $x_u^{(i)}$ are the heights of the heavy fluid surface at the moments when the flow reverses from the ith down to the ith up flow and from the ith up to the $(i+1)$th down flow, respectively. $x_{d0}^{(i)}$ and $x_{u0}^{(i)}$ are the asymptotic values for the exponential curves fitted to the ith down and up flow, respectively (see Fig. 4). In the present analysis, we have averaged the data over four cycles from the second to the fifth in a series of experiments. In fact, s_d and s_u are expected to be suitable parameters for qualifying the timing of the flow reversal over the entire process leading to the asymptotic equilibrium, because $x_{d0}^{(i)}$ and $x_{u0}^{(i-1)}$ are thought to be almost consistent with the hydrostatic equilibrium where the pipe filled

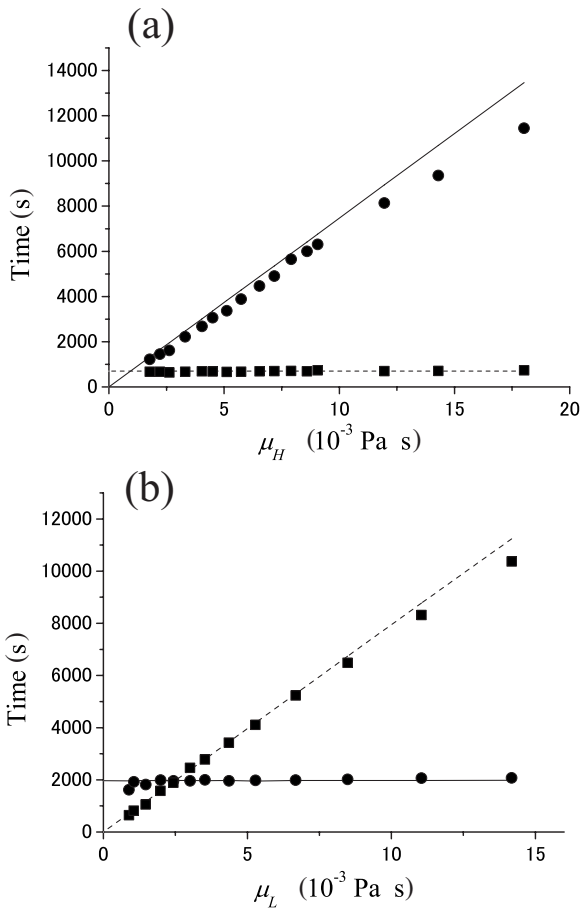

FIG. 7. Time constants of the exponential curves fitted for each down and up flow (filled circle and squares, respectively). The data are averaged over four cycles from the second to the fifth. (a) μ_H is varied while μ_L is fixed at 0.89×10^{-3} Pa s. (b) μ_L is varied while μ_H is fixed at $(2.63\pm0.03)\times10^{-3}$ Pa s. The solid and dashed lines indicate the theoretical lines for τ_d and τ_u, respectively.

with heavy and light fluids $x_{de}^{(i)}$ and $x_{ue}^{(i-1)}$, respectively, with a density difference of $\delta\rho^{(i)}$. Figure 8 shows the viscosity dependence of s_d and s_u when the viscosity of either the heavy or light fluid is varied. It is clear that both s_d and s_u increase when the viscosity of the heavy fluid increases, but decrease when that of the light fluid increases. These results cannot be explained in terms of previous theories, in which the critical heights do not depend on the viscosity [19].

Thus, it becomes clear that the flow-reversal process is significantly affected by the viscosity of the fluid. In order to investigate this phenomenon in greater detail, we observed the flow reversal from the down to up flow using a stereomicroscope. An example of the result is shown in Fig. 9. At first, an intrusion of the light fluid into the pipe is observed long before the actual moment of the flow reversal and it grows upward rather slowly [Fig. 9(b)]. When the intrusion length measured from the bottom of the pipe becomes nearly 1 mm, it suddenly starts to grow rapidly [Figs. 9(c) and 9(d)], and finally, the flow reverses. It is surprising that the temporal evolution of the effective flow volume through a pipe and hence that of the height of the heavy fluid surface still obey an exponential response during the gradual growth

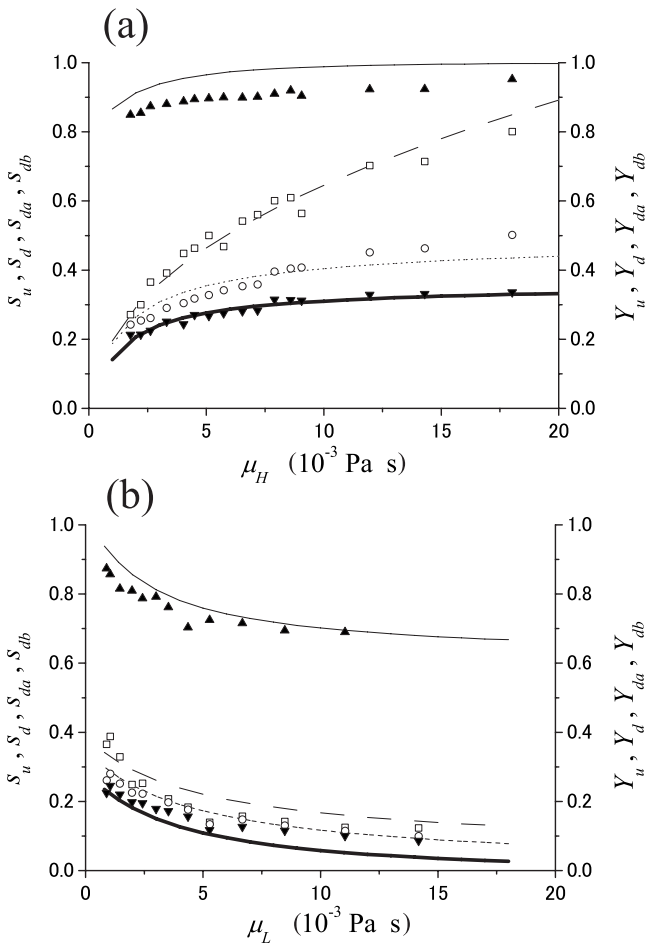

FIG. 8. Viscosity dependence of s_u (filled up triangles), s_d (filled down triangles), s_{da} (open squares), and s_{db} (open circles). The data are averaged over four cycles from the second to the fifth. Simulated results Y_u (solid lines), Y_d (bold lines), Y_{da} (dashed lines), and Y_{db} (dotted lines) are also shown. (a) μ_H is varied while μ_L is fixed at 0.89×10^{-3} Pa s. (b) μ_L is varied while μ_H is fixed at $(2.63\pm0.03)\times10^{-3}$ Pa s. The parameters of the simulation are as follows: $c=800$ N m^{-3}, $k=4.00\times10^4$ m^{-1} s^{-1}, $\alpha=1.82$, $\gamma=0.30$, $\rho_L=0.997\times10^3$ kg m^{-3}, $\delta\rho=0.061\times10^3$ kg m^{-3}, $g=9.80$ m s^{-2}, $b_2=8.76\times10^5$ m^{-1}, and $r=7.89\times10^8$ m^{-2} s^2.

of the intrusion. Even after the intrusion starts to grow rapidly, the deviation from an exponential curve is negligibly small, compared with the amplitude of the oscillation (see Fig. 4).

The above behavior is found to depend significantly on the viscosity of the fluid. Figure 10 shows the temporal evolution of the intrusion length when the viscosity of either heavy or light fluid is varied. Here, we set the origin of time to be at the very moment of the flow reversal and plot the intrusion length against the time leading to the flow reversal. For a large μ_H and small μ_L, the intrusion of the light fluid persists an extremely long time before the flow reversal occurs, and the growth rate during the rapid-growing process is also relatively small, as shown in Fig. 10(a). On the other hand, for a large μ_L and small μ_H, the growth rate of the intrusion is relatively large and essentially does not depend on μ_L [Fig. 10(b)]. However, in the latter case, it is observed

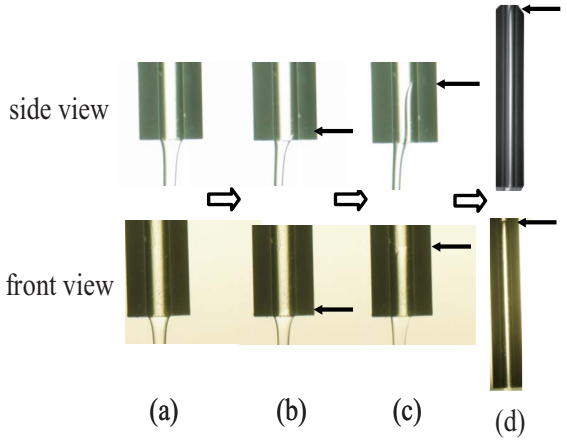

FIG. 9. (Color online) Microscopic images of the intrusion in the time course of down flow [(a)→(b)→(c)→(d)]. Upper and lower images show the side and front views, respectively. An intrusion of light fluid is clearly seen (arrows). Glucose solution and water are used as the heavy and light fluids, respectively. $\rho_L=0.997\times10^3$ kg m^{-3}, $\delta\rho=0.067\times10^3$ kg m^{-3}, $\mu_H=1.42\times10^{-3}$ Pa s and $\mu_L=0.89\times10^{-3}$ Pa s. Although the experimental condition employed in this figure is slightly different from that employed in the text, the difference is not crucial, as the behavior observed is almost identical.

that the interface between the two fluids is somehow disturbed at a certain intrusion length and its growth is thus obstructed for some time, particularly at a large μ_L. A typical example is shown in Fig. 11. In addition to the intrusion length, its width within the pipe depends on the viscosity of the fluids, as shown in Fig. 12. In general, the width is larger for $\mu_H>\mu_L$, while it is smaller for $\mu_H<\mu_L$.

We characterize the viscosity-dependent behavior of the intrusion by employing the following two quantities:

$$s_{da}=\left\langle\frac{x_{da}^{(i)}-x_{d0}^{(i)}}{x_{u0}^{(i-1)}-x_{d0}^{(i)}}\right\rangle,$$

$$s_{db}=\left\langle\frac{x_{db}^{(i)}-x_{d0}^{(i)}}{x_{u0}^{(i-1)}-x_{d0}^{(i)}}\right\rangle, \tag{11}$$

where $x_{da}^{(i)}$ and $x_{db}^{(i)}$ are the heights of the heavy fluid surface at the time when the intrusion lengths exceed 0.1 and 1 mm, respectively. Because the intrusion begins to grow rapidly when its length becomes nearly 1 mm, as shown in Fig. 10, the two quantities s_{da} and s_{db} roughly characterize the timings for the beginning of the intrusion and for the onset of its rapid growth, respectively. With increasing μ_H, significant increases in both s_{da} and s_{db} are observed, which are more remarkable than those of s_d [Fig. 8(a)]. Thus, the clear sign of the flow reversal is expressed, which is more prominent with increasing μ_H. On the other hand, with increasing μ_L, the behaviors of s_{da} and s_{db} are similar to those of s_d [Fig. 8(b)]. Thus, these newly introduced quantities characterize the dynamics of the flow reversal fairly sensitively and then clarify definitively the viscosity dependence of the density oscillation.

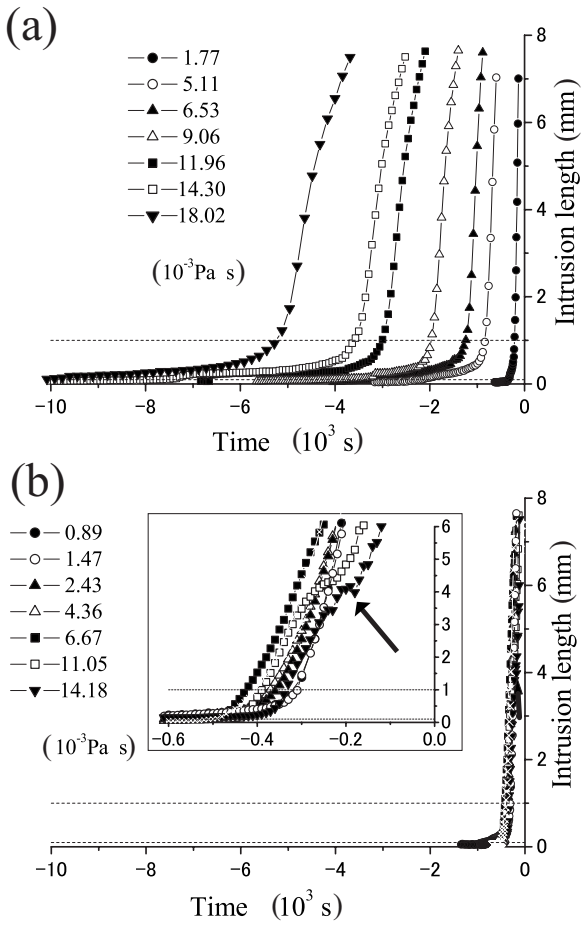

FIG. 10. Viscosity-dependent temporal evolution of the intrusion of light fluid. (a) μ_H is varied while μ_L is fixed at 0.89×10^{-3} Pa s. (b) μ_L is varied while μ_H is fixed at $(2.63 \pm 0.03) \times 10^{-3}$ Pa s. Because of the limitation of the visual field under the stereomicroscope, an intrusion length of more than 8 mm is not observed. The dotted lines indicate 0.1 and 1 mm of intrusion length. The inset in (b) shows an enlarged view. The obstruction of the growth is observed at a large μ_L (shown as an arrow, see also Fig. 11).

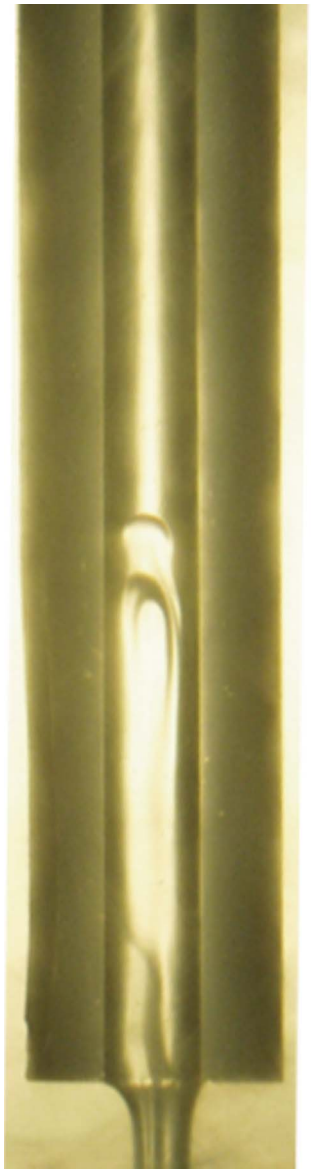

FIG. 11. (Color online) Front view of the disturbance of the interface at a large μ_L. $\mu_H = 2.66 \times 10^{-3}$ Pa s and $\mu_L = 14.18 \times 10^{-3}$ Pa s.

V. ANALYSES AND DISCUSSION

The viscosity dependence of the flow reversal observed above is helpful in understanding the fundamental mechanism of density oscillation. Unfortunately, an exact treatment of flow stability is difficult owing to the complexity of the flow within the pipe during the flow-reversal process. Thus, a simple model describing the essential mechanism of the flow-reversal process is required. In this section, we will propose the model for down to up flow by considering only forces parallel to the pipe wall, which act on a unit volume element located at the tip of the intrusion. Here, we consider only the case where the pipe length is much larger than the diameter and the nonlinear term in Eq. (1) is neglected, i.e., $\beta \sigma_i^{1/2}/4 \ll 1$. We will show at the end of this section that the experimental result is quantitatively reproducible by this model.

Now, let us consider the forces concerned with this phenomenon separately. First, there should be a viscous drag force F_1 acting on the interface between the heavy and light fluids. Actually, a definite interface between these two fluids will not exist, since the viscosity of the fluid will vary continuously in space because of the miscible nature of the heavy and light fluids. For convenience, however, we consider that the mixed region consists of an extremely thin volume element at an interface with a fluid having an appropriate viscosity. Since the viscosity of the fluid at the interface μ_{int} may be somehow dependent on the viscosities of the two fluids, for simplicity, we write $\mu_{\text{int}} = (\mu_H + \mu_L)/2$. The drag force F_1 should depend both on the viscosity of the fluid and on the velocity gradient at the interface, the latter of which is in proportion to the difference between the velocity of down flow and the growth rate of the intrusion. Thus, F_1 is described as

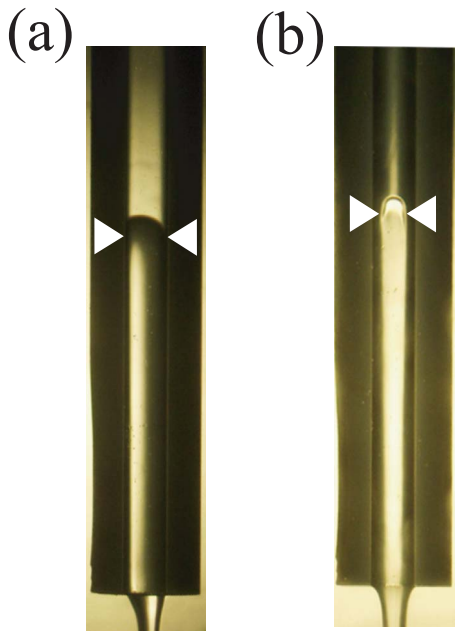

FIG. 12. (Color online) Front views of the intrusions during the flow-reversal processes for (a) $\mu_H=18.02\times10^{-3}$ Pa s and $\mu_L=0.89\times10^{-3}$ Pa s, and (b) $\mu_H=2.65\times10^{-3}$ Pa s and $\mu_L=8.48\times10^{-3}$ Pa s. The width of the intrusion is larger in (a) than in (b) (white arrow heads).

$$F_1=\frac{\mu_H+\mu_L}{2}(b_1\dot{Y}-b_2\dot{\Xi}), \tag{12}$$

where b_1 and b_2 are positive constants. $\Xi\equiv\xi/a$ denotes the nondimensionalized intrusion length with ξ the intrusion length measured from the bottom of the pipe. Y is defined using $x_{ue}^{(i-1)}$ and $x_{de}^{(i)}$, values at two hydrostatic equilibria, as

$$Y\equiv\frac{(x-x_{de}^{(i)})}{(x_{ue}^{(i-1)}-x_{de}^{(i)})}\approx\frac{(\rho_L+\delta\rho)}{\rho_L}X \tag{13}$$

(see Fig. 13), and thus, its derivative characterizes the velocity of the down flow. It is noticed that the intrusion must be resisted not only by the viscous drag at the interface between the fluids, but also by the pipe wall. Since we take the latter effect into the second term on the right-hand side of Eq. (12), for simplicity, b_1 and b_2 are considered as independent parameters. Here, using Eq. (5), $\dot{Y}$ in Eq. (12) can be replaced by $-Y/\nu_H r$, under the assumption that Eq. (1) holds until the very moment of the flow reversal from the down to up flow. This assumption is thought to be valid because the deviation from an exponential curve in the height of the heavy fluid surface is found to be sufficiently small as compared with the amplitude of the oscillation until the flow reversal is completed. Thus, Eq. (12) is rewritten as

$$F_1=-\frac{c(\mu_H+\mu_L)}{2}\frac{Y}{\mu_H}-\frac{b_2(\mu_H+\mu_L)}{2}\dot{\Xi}, \tag{14}$$

where $c\equiv b_1(\rho_L+\delta\rho)/r$.

Second, there must be a gravitational force and the force due to the gradient of hydrostatic pressure. We denote such hydrostatic forces as F_2. When the intrusion exists sufficiently at the interior of the pipe, F_2 will satisfy the relation

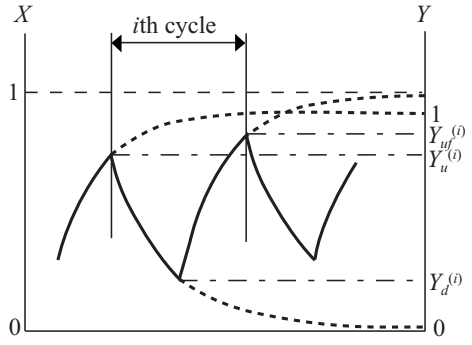

FIG. 13. Definition of the parameters denoting the height of the heavy fluid surface at the ith cycle. The dotted lines denote exponential curves fitted for the up and down flows, and the dashed lines denote their asymptotic values. The dashed and dotted lines denote the heights when the flow reverses from up (down) to down (up) flow.

$$F_2=-\frac{P_u-P_d}{d}-\rho_L g,$$

where P_u and P_d denote the hydrostatic pressures at the upper and lower ends of the pipe, and the gradient of the hydrostatic pressure is assumed to be homogeneous inside the pipe. Then, if we assume that P_u and P_d are simply derived from the heights of the fluid surfaces as $(\rho_L+\delta\rho)g(x-d)$ and $\rho_L gh$, respectively, F_2 becomes $\delta\rho g(1-Y)$. On the other hand, if the volume element of the light fluid exists outside the pipe, it is obvious that the hydrostatic pressure gradient balances the gravitational force. Hence, when there is no intrusion ($\Xi=0$), the relation $F_2=0$ should be automatically satisfied. Since F_2 is thought to be a continuous function of Ξ, it seems appropriate to describe F_2 in the following way:

$$F_2=\delta\rho g(1-Y)(1-e^{-\Xi/\alpha}). \tag{15}$$

The term $(1-e^{-\Xi/\alpha})$ is introduced in order to connect $F_2=\delta\rho g(1-Y)$ for $\Xi\gg\alpha$ and $F_2=0$ for $\Xi=0$. Here, α characterizes the spatial range where F_2 takes a value between 0 and $\delta\rho g(1-Y)$.

Third, we consider the effect of the acceleration of the fluid outside the pipe. Let us arbitrarily consider two planes inside and outside the pipe as PL_1 and PL_2, as shown in Fig. 14. We define the absolute values of the mean velocities of the flows at PL_1 and PL_2 as V_1 and V_2, respectively, where $V_1\propto-\dot{Y}\propto Y/\mu_H$ is obtained from Eq. (5). Since the heavy fluid that has passed through the pipe is accelerated due to the hydrostatic pressure gradient, the following relation is expected to hold:

$$V_2=V_1+\kappa, \tag{16}$$

where κ expresses the effect of the acceleration. The continuity condition naturally holds, which results in

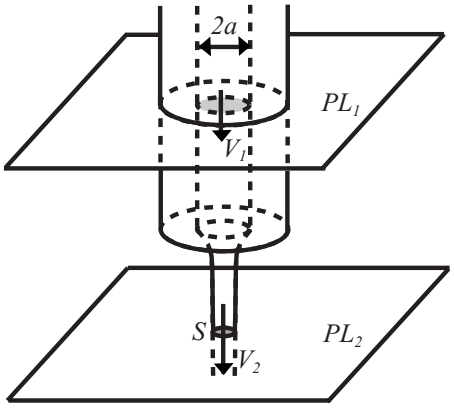

FIG. 14. Schematic illustration of two planes PL_1 and PL_2, which are vertical to the direction of the flow. PL_1 crosses the pipe, while PL_2 is below but not too far from the lower end of the pipe. S denotes the surface area of down flow at PL_2. V_1 and V_2 are the mean velocities of the down flow at PL_1 and PL_2, respectively.

$$V_1 \pi a^2 = V_2 S, \tag{17}$$

where S denotes the cross section of the down flow at PL_2. When S is sufficiently small, it is expected that the intrusion of the light fluid is enforced as a consequence, because the contraction of the flow causes a detachment of the down flow from the pipe wall. F_3 is defined as the force due to this enforcement. By substituting $V_1 \propto Y/\mu_H$ into Eqs. (16) and (17), we find that $(\pi a^2/S-1) \propto \mu_H/Y$. Since F_3 increases as S decreases, F_3 should increase as μ_H/Y increases. In addition, F_3 is also expected to be large when Ξ is small. Therefore, F_3 is phenomenologically described as

$$F_3 = k e^{-\Xi/\gamma} \frac{\mu_H}{Y}, \tag{18}$$

where k is a positive constant. γ expresses the spatial range where the force works effectively. From Eqs. (14), (15), and (18), we can describe the total force F acting on the intrusion as

$$F = F_1 + F_2 + F_3 = f(\Xi) - \frac{b_2(\mu_H + \mu_L)\dot{\Xi}}{2}, \tag{19}$$

where

$$f(\Xi) \equiv -\frac{c(\mu_H + \mu_L)}{2}\frac{Y}{\mu_H} + \delta\rho g(1-Y)(1-e^{-\Xi/\alpha}) + k e^{-\Xi/\gamma}\frac{\mu_H}{Y}. \tag{20}$$

Let us consider the result of gradually decreasing Y. For this purpose, we have performed a numerical simulation. The equation of motion for a unit volume element located at the tip of the intrusion $\rho_L \ddot{\xi} = F$ is rewritten by using Eqs. (19) and (20) as follows:

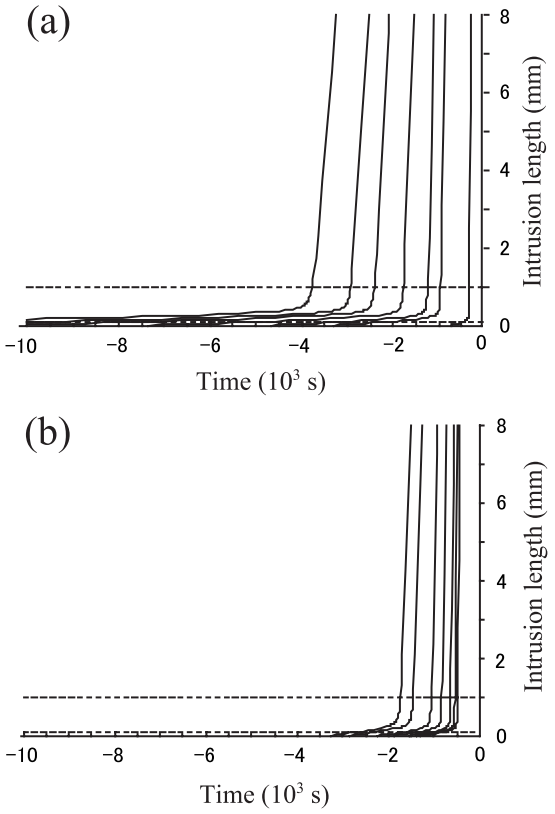

FIG. 15. The viscosity-dependent temporal evolution of the intrusion of light fluid calculated from Eqs. (20)–(22). (a) μ_H is varied while μ_L is fixed at 0.89×10^{-3} Pa s. Each curve corresponds to μ_H=1.77, 5.11, 6.53, 9.06, 11.96, 14.30, and 18.02 ($\times10^{-3}$ Pa s) from right to left, respectively. (b) μ_L is varied while μ_H is fixed at 2.63×10^{-3} Pa s. Each curve corresponds to μ_H=0.89, 1.47, 2.43, 4.36, 6.67, 11.05, and 14.18 ($\times10^{-3}$ Pa s) from right to left, respectively. The dotted lines denote 0.1 and 1 mm of intrusion length. The parameters employed are as follows: c=800 N m^{-3}, k=4.00 $\times10^4$ m^{-1} s^{-1}, α=1.82, γ=0.30, ρ_L=0.997$\times10^3$ kg m^{-3}, $\delta\rho$ =0.061$\times10^3$ kg m^{-3}, g=9.80 m s^{-2}, b_2=8.76$\times10^5$ m^{-1}, and r =7.89$\times10^8$ m^{-2} s^2.

$$\rho_L a \ddot{\Xi} = f(\Xi) - \frac{b_2(\mu_H + \mu_L)}{2}\dot{\Xi}, \tag{21}$$

with Y satisfying the relation

$$\dot{Y} = -\frac{Y}{\tau_d}. \tag{22}$$

Using Eqs. (20)–(22) under the initial condition of $\Xi=\dot{\Xi}=0$ at $Y=Y_c \equiv \sqrt{2k/c\mu_H}/\sqrt{\mu_H+\mu_L}$, we obtain the simulated data as shown in Fig. 15. The values of parameters α, γ, b_2, c, and k have been chosen properly. In this figure, t is redefined so that its origin agrees with the time when the intrusion reaches the upper end of the pipe $\Xi=\lambda\equiv d/a$, which corresponds to the moment when the flow reverses completely. In the present experimental condition, we put λ =191.78. First, let us observe the general trend of the intrusion process. We can see clearly that the intrusion begins long before the flow reversal and grows rather slowly. When

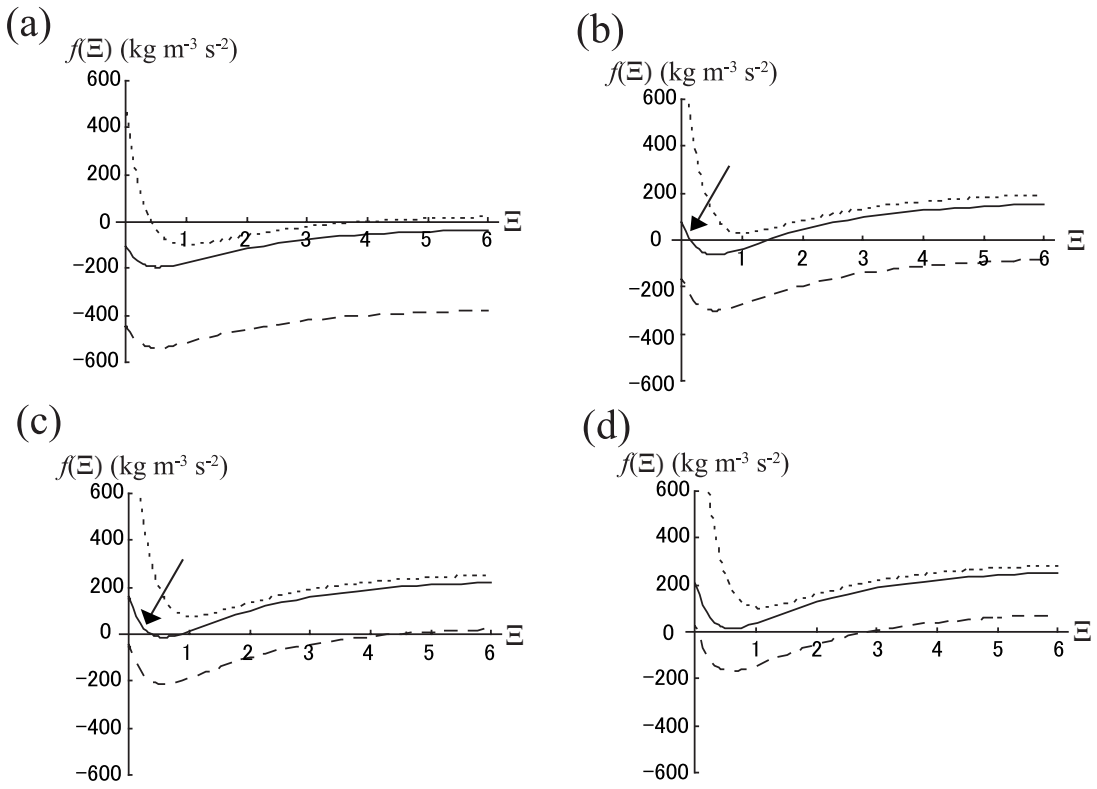

FIG. 16. $f(\Xi)$ for various values of Y: (a) $Y=0.55$, (b) $Y=0.38$, (c) $Y=0.32$, and (d) $Y=0.29$. The solid lines indicate the case for $\mu_H=2.63\times10^{-3}$ Pa s and $\mu_L=0.89\times10^{-3}$ Pa s, the dotted lines indicate the case for $\mu_H=10.00\times10^{-3}$ Pa s and $\mu_L=0.89\times10^{-3}$ Pa s, and the dashed lines indicate the case for $\mu_H=2.63\times10^{-3}$ Pa s and $\mu_L=5.00\times10^{-3}$ Pa s. The parameters employed are as follows: $c=800$ N m^{-3}, $k=4.00\times10^4$ m^{-1} s^{-1}, $\alpha=1.82$, $\gamma=0.30$, $\rho_L=0.997\times10^3$ kg m^{-3}, $\delta\rho=0.061\times10^3$ kg m^{-3}, and $g=9.80$ m s^{-2}. The arrows denote the stable solution of Eq. (20), $\Xi=\Xi_0$.

the intrusion exceeds a certain extent, it suddenly starts to grow rapidly, which agrees quite well with the experimental result (Fig. 10).

The above behavior is easily understandable considering the Y-dependent functional form of $f(\Xi)$ in Eq. (21). Here, it is noticed that Y is a slowly varying variable, as shown in Eq. (22). Figure 16 shows the Y dependence of $f(\Xi)$. Look at the case of $\mu_H=2.63\times10^{-3}$ Pa s and $\mu_L=0.89\times10^{-3}$ Pa s in Fig. 16. In the case of $Y\geq Y_c$, the intrusion does not occur and Ξ remains zero, because the relation $f(0)\leq0$ clearly holds [Fig. 16(a)]. However, when Y becomes less than Y_c, $f(0)$ becomes positive and the relation $f(\Xi)=0$ leads to a positive solution Ξ_0 with $f'(\Xi_0)<0$; hence, $\Xi=\Xi_0$ becomes a stable solution of Eq. (21). Thus, the light fluid begins to intrude into a pipe [Fig. 16(b)]. As Y decreases much more, Ξ_0 increases gradually [Fig. 16(c)] and finally, the solution of $f(\Xi)=0$ vanishes, which leads to $f(\Xi)>0$ for all Ξ [Fig. 16(d)]. Thus, the intrusion becomes accelerated suddenly and the damping term in Eq. (21) becomes balanced with $f(\Xi)$, which leads to $\dot{\Xi}$ being constant. Finally, the flow reverses completely when the tip of the intrusion reaches the upper end of the pipe ($\Xi=\lambda$).

The change in the viscosity of the fluid drastically alters the temporal behavior. When μ_H is increased, while μ_L is kept constant, the intrusion of the light fluid tends to last for an extremely long time before the flow reversal occurs and the growth rate in the rapid-growing region becomes relatively small, as shown in Fig. 15(a); this is in good agreement with the experimental result [Fig. 10(a)]. In the same way as in the experiment, we have defined the parameters Y_{da} and Y_{db} as the values of Y when the intrusion length becomes 0.1 and 1 mm, corresponding to $\Xi=0.27$ and 2.74, which characterize the timings for the beginning of the intrusion and the onset of its rapid growth, respectively. In addition, we have defined Y_d as the value of Y when Ξ becomes λ, which characterizes the timing for the flow reversal. The calculated result is shown in Fig. 8. In spite of the simplest model, Y_{da}, Y_{db}, and Y_d are surprisingly in good agreement with the experimental results of s_{da}, s_{db}, and s_d.

When μ_L is increased, while μ_H is kept constant, overall behaviors are reproduced fairly well. Namely, Y_{da}, Y_{db}, and Y_d decrease as μ_L increases, and their values are nearly consistent with the experimental results, as shown in Fig. 8(b). However, the simulated results [Fig. 15(b)] seem slightly different from the experimental results [Fig. 10(b)] in that the growth rate of the intrusion is generally slower for large μ_L in the simulation than that in the experiment.

Such viscosity dependence of Y_{da}, Y_{db}, and Y_d is easily understood from Fig. 16. For large μ_H, $f(\Xi)$ becomes relatively large, especially for small Ξ, which is mainly due to the contribution of F_3. Thus, the intrusion and hence the onset of its rapid growth occur even when Y is still large. On the other hand, for large μ_L, the value of $f(\Xi)$ generally becomes small because of the large contribution of F_1.

Hence, the intrusion and the onset of its rapid growth occur, when Y becomes sufficiently small.

Thus, the behavior of the flow reversal from down to up flow is reproduced fairly well by the present model. In this model, we have introduced the three forces present during the flow-reversal process. Now we will show which force is dominant among them. When μ_H and μ_L are $O(1)\times 10^{-3}$ Pa s and Y is not too small compared with unity, we find from Eqs. (14), (15), and (18) that the contributions of F_1, F_2, and F_3 are characterized by the parameter values c, $\delta\rho g$, and $k\mu_H$, which are 800, 597.8, and $40\times O(1)$ N m^{-3}, respectively. Thus, the contributions of F_1 and F_2 are of the same order, and F_1 is dominant at large Y, while F_2 is dominant at small Y. The contribution of F_3 is small as compared with F_1 and F_2 in this case. However, when the value of μ_H/Y becomes much larger than $O(1)\times 10^{-3}$ Pa s, F_3 becomes comparable to F_1 and F_2 and causes the intrusion.

The parameters α and γ introduced phenomenologically are keys to the dynamics of the flow-reversal process. They characterize not only the region where the pressure gradient is not simply derived from the height of the fluid surface, but also the intrusion length where the onset of its rapid growth occurs. Since the characteristic length of this region is thought to be of the order of the pipe diameter, it is expected that the values of α and γ are $O(1)$. Actually, the values we set to fit the experimental result, i.e., $\alpha=1.82$ and $\gamma=0.30$, are within this order.

The flow reversal from up to down flow is considered in the same manner (Appendix), although the analysis becomes somewhat complicated because the decrease in the density of the heavy fluid due to inflow of the light fluid into the inner container must be taken into account. The viscosity dependence of Y_u thus calculated is also shown in Fig. 8, where we define the value of Y at the moment when the ith down flow begins as $Y_u^{(i)}$ (see Fig. 13). We can see that Y_u is qualitatively in good agreement with the experimental value s_u, although Y_u is slightly larger than s_u for $\mu_H > \mu_L$.

In the above experiment and analysis, we have shown that the behavior of the flow reversal is well described by the present model. Thus, it is clear that this model contains the essential part of the flow-reversal process. Here, we comment on several discrepancies found between the simulation and the experiment. The first is the growth rate of the intrusion in the case of $\mu_L > \mu_H$ at the flow reversal from down to up flow, in which the simulated data are somewhat slower than in the experiment, with the result that Y_d becomes slightly smaller than s_d. This is thought to be closely related to the actual width of the intrusion within the pipe. As described above, it is found experimentally that the width of the intrusion is smaller for $\mu_L > \mu_H$ (Fig. 12). As the width becomes smaller, the resistance to the growth of the intrusion tends to decrease, which enables the intrusion to grow more rapidly. The reason for the relatively slow growth rate in the simulation is thought to be due to the neglect of this effect. The fact that Y_u is slightly larger than s_u for $\mu_H > \mu_L$ is considered in the same way for the opposite flow reversal. However, the reason that the width depends on the viscosities of the fluids is not yet clear. The second discrepancy is connected with the obstruction of the growth due to a disturbance of the interface (Fig. 11), which is observed in the experiment but is not reproduced in the simulation. This phenomenon seems to be due to some kind of hydrodynamic instability at the interface.

Finally, we will briefly mention some effects that possibly relate to the flow-reversal process. First, the interfacial tension between the fluid and the pipe wall may affect the flow-reversal process. Actually, when the proportions of water, one-propanol, and glycerin are varied in the experiment, not only the viscosity but also the interfacial tension varies. However, from the present experiment and analysis, the main cause for the change in the flow-reversal process is thought to be due to the viscosity of the fluids, since we have confirmed that similar results for s_d and s_u are obtainable even when a pair of solutions such as glucose solution and water are employed, in which methyl-cellulose is dissolved to change the viscosity.

Second, the length and diameter of a pipe will relate to the flow-reversal process. We have experimentally confirmed that our model is valid even when the pipe length is varied as far as it is sufficiently larger than the pipe diameter, i.e., $\lambda \gg 1$, and also the nonlinear term in Eq. (1) is negligible. Otherwise, our model no longer holds or needs to be modified, because it is expected that the flow inside the pipe tends to lose its stability even by a slight intrusion when λ is comparable to α and γ. Additionally, the parameters c, b_2, and k will depend on the diameter of the pipe. Third, the density difference between the heavy and light fluids will also affect the flow-reversal process. We have experimentally observed that the growth of the intrusion becomes slower as $\delta\rho$ decreases, and that the temporal evolution of the heavy fluid surface clearly deviates from an exponential curve during each flow-reversal process when $\delta\rho$ is extremely small. Thus, further investigation is clearly needed.

From the above experiment and analysis, we have shown that the flow-reversal process begins with an intrusion of the fluid and is followed by its rapid growth. This process is found to be definitely sensitive to the viscosities of the fluids, although the previous study implied that the critical heights do not depend on the viscosities of the fluids [19]. This is because the force F_3, which plays the role of the "trigger" of the intrusion, depends on the viscosity of the fluid. Moreover, the viscous drag force F_1 is directly connected to the viscosity of the fluid at the interface μ_{int} and the velocity of down (up) flow V_1, both of which are clearly viscosity dependent. Thus, the present model that takes account of the viscosity dependence provides an absolutely important aspect of the flow reversal which has never been considered before.

VI. SUMMARY

In conclusion, we have shown through detailed experiments that the behavior of the flow reversal is definitely sensitive to the viscosities of the fluids, and the experimental results are well explained by a simple model that takes into account the forces acting on a unit volume element located at the tip of the intrusion. Although the previously reported models described the behavior of oscillation phenomenologi-

cally [11–13], they did not explicitly take into account the flow-reversal process, which is the most essential process in the density oscillator and, thus, the fundamental mechanism of the oscillation was not truly understood. We have clarified the essential mechanism of the density oscillator by considering three forces acting on the intrusion into a pipe connecting the light and heavy fluids. Thus, the approach from a microscopic viewpoint will lead us to "truly" understand the mechanisms of nonlinear dynamical systems.

APPENDIX

The temporal evolution of the intrusion during the flow reversal from up to down flow is described in the same way as Eqs. (20)–(22):

$$(\rho_L + \delta\rho)\ddot{\Xi}' = f(\Xi') - \frac{b_2(\mu_H + \mu_L)}{2}\dot{\Xi}', \tag{A1}$$

$$f(\Xi') = \frac{c(\mu_H + \mu_L)}{2}\frac{1-X}{\mu_L} - \delta\rho g X(1 - e^{\Xi'/\alpha}) - ke^{\Xi'/\gamma}\frac{\mu_L}{1-X}, \tag{A2}$$

$$\dot{X} = \frac{1-X}{\tau_u}. \tag{A3}$$

Here, $\Xi' = \xi'/a$ and ξ' is defined as the intrusion length measured from the upper end of the pipe, where the upper direction is taken as positive. Hence, Ξ' takes a negative value when a heavy fluid intrudes. Further, under the assumption of $x_{ue}^{(i-1)} - x_u^{(i-1)} = x_{ue}^{(i)} - x_u^{(i)}$, the following relation is derived:

$$Y_{uf}^{(i)} - Y_u^{(i)} = \frac{x_u^{(i)} - x_u^{(i-1)}}{\delta x^{(i)}} = \frac{x_{ue}^{(i)} - x_{de}^{(i)} - \delta x^{(i)}}{\delta x^{(i)}} = \frac{\delta\rho^{(i)}}{\rho_L}, \tag{A4}$$

where $Y_{uf}^{(i)}$ denotes the value of Y when flow reverses from the ith up flow to $(i+1)$th down flow (see Fig. 13). Then, since Y_{uf} is derived numerically from Eqs. (A1)–(A3) by using Eq. (13), we can derive Y_u using Eq. (A4).

[1] M. V. L. Bennett and R. S. Zukin, Neuron **41**, 495 (2004).
[2] J. C. Dunlap, Cell **96**, 271 (1999).
[3] B. Blasius, R. Neff, F. Beck, and U. Lüttge, Proc. R. Soc. London, Ser. B **266**, 93 (1999).
[4] A. Kuznetsov, M. Kærn, and N. Kopell, SIAM J. Appl. Math. **65**, 392 (2004).
[5] R. J. Field and R. M. Noyes, J. Chem. Phys. **60**, 1877 (1974).
[6] K. Wiesenfeld, P. Colet, and S. H. Strogatz, Phys. Rev. E **57**, 1563 (1998).
[7] Y. Kuramoto, *Chemical Oscillations, Waves, and Turbulence* (Springer-Verlag, Berlin, 1984).
[8] A. Pikovsky, M. Rosenblum, and J. Kurths, *Synchronization: A Universal Concept in Nonlinear Sciences* (Cambridge University Press, Cambridge, 2001).
[9] P. S. Landa, *Nonlinear Oscillations and Waves in Dynamical Systems* (Kluwer Academic Publishers, Dordrecht, 1996).
[10] S. Martin, Geophys. Fluid Dyn. **1**, 143 (1970).
[11] K. Yoshikawa and H. Kawakami, Oyo Suri **4**, 238 (1994).
[12] K. Yoshikawa and K. Fukunaga, Chem. Phys. Lett. **174**, 203 (1990).
[13] K. Yoshikawa, S. Maeda, and H. Kawakami, Ferroelectrics **86**, 281 (1988).
[14] M. Okamura and K. Yoshikawa, Phys. Rev. E **61**, 2445 (2000).
[15] S. Nakata, T. Miyata, N. Ojima, and K. Yoshikawa, Physica D **115**, 313 (1998).
[16] K. Miyakawa and K. Yamada, Physica D **151**, 217 (2001).
[17] K. Miyakawa and K. Yamada, Physica D **127**, 177 (1999).
[18] K. Yoshikawa, N. Oyama, M. Shoji, and S. Nakata, Am. J. Phys. **59**, 137 (1991).
[19] O. Steinbock, A. Lange, and I. Rehberg, Phys. Rev. Lett. **81**, 798 (1998).
[20] M. Ueno, F. Uehara, Y. Narahara, and Y. Watanabe, Jpn. J. Appl. Phys., Part 1 **45**, 8928 (2006).
[21] G. I. Taylor, Proc. R. Soc. London, Ser. A **201**, 192 (1950).
[22] P. G. Saffman and G. I. Taylor, Proc. R. Soc. London, Ser. A **245**, 312 (1958).
[23] R. Menikoff, R. C. Mjosness, D. H. Sharp, and C. Zemach, Phys. Fluids **20**, 2000 (1977).
[24] In the present paper, superscript (i) is omitted when it is not essential.